Journal of the American Heart Association

ORIGINAL RESEARCH

Imaging of Angiogenesis in White Matter Hyperintensities

Lingling Ding, MD; Bo Hou, MD; Jie Zang, PhD; Tong Su, MD; Feng Feng, MD; Zhaohui Zhu, MD; Bin Peng, MD

BACKGROUND: White matter hyperintensities (WMHs) are areas of increased signal intensity on T2-weighted magnetic resonance imaging (MRI). WMH penumbra may be a potential target for early intervention in WMHs. We explored the relationship between angiogenesis and WMH penumbra in patients with WMHs.

METHODS AND RESULTS: Twenty-one patients with confluent WMHs of Fazekas grade ≥2 were included. All the participants underwent ^{68}Ga-NOTA-PRGD2 positron emission tomography/magnetic resonance imaging. WMH penumbra was analyzed with masks created for the WMH and 7 normal-appearing white matter layers; each layer was dilated away from the WMH by 2 mm. Angiogenesis array and ELISA were used to detect the serum levels of angiogenic factors, inflammatory factors, HIF-1 alpha, and S100B. Fourteen patients with increased ^{68}Ga-NOTA-PRGD2 maximum standardized uptake (>0.17) were classified into group 2. Seven patients with maximum standardized uptake ≤0.17 were classified as group 1. WMH volume and serum levels of integrin αvβ3, vascular endothelial growth factor receptor 22, and interleukin-1β tended to be higher in group 2 than in group 1. In group 2, ^{68}Ga-NOTA-PRGD2 uptake was significantly increased at the border between the WMH and normal-appearing white matter than in WMHs (P=0.004). The structure penumbra, defined by fractional anisotropy, was wider in group 2 (8 mm) than in group 1 (2 mm). The cerebral blood flow penumbra was 12 mm in both groups. Angiogenesis showed a correlation with reduced cerebral blood flow and microstructure integrity.

CONCLUSIONS: Our study provides evidence that angiogenesis occurs in the WMH penumbra. Further studies are warranted to verify the effect of angiogenesis on WMH growth.

Key Words: angiogenesis ■ cerebral blood flow ■ PET/MRI ■ white matter hyperintensities

White matter hyperintensities (WMHs) are part of the spectrum of cerebral small-vessel disease markers, which are considered age-specific changes in magnetic resonance imaging (MRI) and extend over time.[1] In recent years, an increasing number of studies have observed the impact of WMH progression on predicting a more rapid decline in global cognitive performance.[2,3] Sabayan et al[4] found an association between accelerated progression of WMHs and a high risk of all-cause death (hazard ratio, 1.22 [95% CI, 1.09–1.37] per mL/y increase in WMHs). Therefore, preventing or slowing the progression of white matter injury has emerged as a major goal of current research.

The term *white matter hyperintensity penumbra* has been used to characterize the normal-appearing white matter (NAWM) tissue surrounding the WMHs and may represent subtle white matter injuries associated with the progression of WMHs. Previous diffusion tensor imaging (DTI) studies have shown that structural WMH penumbra, as measured by fractional anisotropy (FA), extends ≈2 to 9 mm distal to WMH, whereas the cerebral blood flow (CBF) WMH penumbrae are ≈11 to 14 mm distal to WMH. The WMH penumbra has

Correspondence to: Bin Peng, MD, Department of Neurology, Peking Union Medical College Hospital, Chinese Academy of Medical Science and Peking Union Medical College, No. 1, Shuaifuyuan, Dongdan, Dongcheng District, Beijing 100730, China. Email: pengbin3@hotmail.com

This manuscript was sent to Luciano A. Sposato, MD, MBA, FRCPC, Associate Editor, for review by expert referees, editorial decision, and final disposition.

For Sources of Funding and Disclosures, see page 11.

JAHA is available at: www.ahajournals.org/journal/jaha

CLINICAL PERSPECTIVE

What Is New?

- ^{68}Ga-NOTA-PRGD2 positron emission tomography can be used to detect the expression of integrin αvβ3, a molecular biomarker for angiogenesis.
- Our study provides evidence that angiogenesis exists in white matter hyperintensity penumbra.

What Are the Clinical Implications?

- Angiogenesis is correlated with reduced cerebral blood flow and microstructural integrity.
- This study provides new insights into angiogenesis as a novel target for therapeutic intervention to arrest the progression of white matter hyperintensities.

Nonstandard Abbreviations and Acronyms

CBF	cerebral blood flow
DTI	diffusion tensor imaging
FA	fractional anisotropy
FOV	field of view
MD	mean diffusivity
MMP	matrix metalloproteinase
NAWM	normal-appearing white matter
SUV_{max}	maximum standardized uptake values
SUV_r	standardized uptake value ratios
TE	echo time
TR	repetition time
WMHs	white matter hyperintensities

an increased likelihood of conversion to WMHs.[5–8] Therefore, we hypothesized that the WMH penumbra is likely to become a potential target for early intervention in WMHs.

WMH remains a clinical challenge due to its poorly understood pathogenesis. WMHs are thought to have an ischemic pathogenesis caused by chronic hypoperfusion due to localization in the watershed areas formed by the terminal arteries.[9,10] Reduced CBF in the WMH penumbra has been associated with the development of WMHs.[11] Potential interventions to increase white matter blood flow for the prevention of further white matter damage and their clinical consequences have been discussed. Collateral revascularization in the penumbra areas has been correlated with recovery and longer survival times in patients with ischemic stroke.[12,13] Angiogenesis is a form of collateral circulation and a crucial restorative mechanism under ischemic conditions. Recently, several studies have demonstrated a relationship between angiogenic factors and WMHs.[14,15]

Whether angiogenesis exists and plays a role in the WMH penumbra is unclear. There are still challenges in the study of angiogenesis in vivo. However, because positron emission tomography (PET) imaging is widely used in cerebrovascular studies, previous PET studies have shown that arginine–glycine–aspartic acid uptake is significantly correlated with integrin αvβ3 expression and microvessel density. The integrin αvβ3-targeted arginine–glycine–aspartic acid sequence-based probe showed high specificity for angiogenesis imaging.[16–18] ^{68}Ga-NOTA-PRGD2 PET has been used to evaluate angiogenic activity in cerebral ischemic diseases and cancer.[19,20]

In this study, we hypothesized that angiogenesis in the WMH penumbra may be correlated with reduced CBF and white matter integrity. We tested this hypothesis by detecting integrin αvβ3 expression using simultaneous ^{68}Ga-NOTA-PRGD2 PET/MRI.

METHODS

Data Availability

The data that support the findings of this study are available from the corresponding author upon reasonable request.

Study Design and Participants

Twenty-one participants with cerebral small-vessel disease from Peking Union Medical College Hospital between November 2016 and February 2018 were included. The inclusion criterion was confluent WMHs of Fazekas grade ≥2 on MRI. The patients with any cause of WMHs other than small-vessel disease, tumors, systemic inflammatory disease, brain trauma, and contraindications to PET/MRI were excluded. This study was approved by the institutional review board of Peking Union Medical College Hospital. Written informed consent was obtained from all included patients or their representatives.

PET/MRI Protocol

All images were acquired using an integrated time-of-flight (TOF) PET/MRI scanner (SIGNA PET/MRI; GE Healthcare, Waukesha, WI). ^{68}Ga-NOTA-PRGD2 was synthesized as described previously.[21] A dynamic PET scan was performed for 60 minutes after an intravenous injection of ^{68}Ga-NOTA-PRGD2, at a dose of 1.85 MBq (0.05 mCi) per kilogram of body weight. The interval between injection and scanning was about 30 to 60 minutes. PET and 3T MRI data were simultaneously acquired. The magnetic resonance sequences were performed as below: T2-weighted imaging with fast recovery fast spin echo (repetition time [TR]=4691 ms, echo time [TE]=89 ms, field of view [FOV]=22×22 cm, slice thickness=3 mm, slice spacing=0 mm, and matrix=320×320); T1-weighted imaging with 3-dimensional fast spoiled gradient echo (TR=7.4 ms, TE=3.2 ms, preparation time=4.00 ms, number of excitations=1.00, FOV=25.6 cm×23.2 cm, slice thickness=1 mm, slice spacing=0.6 mm, and matrix=256×232); 3-dimensional pseudocontinuous arterial spin labeling (TR=4790 ms, TE=10.2 ms, post label delay (PLD) =)=2025 ms, number of excitations=5, FOV=24 cm×24 cm, slice thickness=5 mm, slice spacing=0 mm, and matrix=320 × 224); fluid attenuated inversion recovery (TE= =130 ms, TR=12 000 ms, time of inversion =) =2711 ms, number of excitations= =2.00, FOV= =21 cm×18.9 cm, slice thickness=3 mm, slice spacing=0 mm, and matrix=256 × 192); and DTI sequence (TR=10 999 ms, TE=72.9 ms, slice thickness=2.5 mm, FOV=24 cm, and 15 diffusion-weighted directions with b=1000 s/mm^2).

Imaging Analysis

To calculate the uptake of ^{68}Ga-NOTA-PRGD2 more precisely, PET images were reconstructed using the time-of-flight method and postprocessed using the GE Advantage Workstation version 4.6 (GE Healthcare). In this study, images were reconstructed using the ordered subset expectation maximization reconstruction method (32 subsets, 8 iterations, filter cutoff frequency of 1.5 mm) combined with high definition (Sharp IR). The full width at half maximum of the Gaussian time-of-flight kernel with a width of 400 ps was used in the reconstruction. Magnetic resonance attenuation correction was performed on the basis of the double-point Dixon sequence.[22]

PET/MRI fusion images were visually evaluated for focal ^{68}Ga-NOTA-PRGD2 uptake by 2 experts. The maximum standardized uptake values (SUV_{max}) were obtained for ^{68}Ga-NOTA-PRGD2 PET images. The participants were divided into 2 groups according to ^{68}Ga-NOTA-PRGD2 SUV_{max} in the WMH, NAWM, or border between the WMH and NAWM.

Tissue Segmentation and Spatial Normalization

CBF maps of arterial spin labeling were generated on a GE AW 4.5 workstation using a software 3-dimensional ASL Functool kit. The model used for calculating CBF (mL/min per 100 g) was based on a previous study.[23]

DTI images were postprocessed using the FMRIB Software Library (FSL version 5.0; http://www.fmrib.ox.ac.uk/fsl). We calculated DTI parameters including FA and mean diffusivity (MD). To further investigate the correlation between ^{68}Ga-NOTA-PRGD2 uptake and changes in CBF (mL/min per 100 g tissue) and white matter structural integrity, all PET-MRI images were preprocessed using SPM12 (statistical parametric mapping; https://www.fil.ion.ucl.ac.uk/spm/software/spm12/). Each image was checked to ensure common orientation.

Fluid attenuated inversion recovery and 3-dimensional T1-weighted images were aligned using affine coregistration for each individual. Three-dimensional T1 images were used to segment brain tissue into cortical gray matter, white matter, and cerebrospinal fluid. WMH lesions were obtained from the 3-dimensional T1- and T2-weighted fluid attenuated inversion recovery images using the Lesion Segmentation Tool in SPM12. Manual refinement was performed by an expert to ensure an accurate representation of WMH using ITK-SNAP (www.itksnap.org). NAWM masks were created for each individual to determine the WMH penumbra for each measure. Each layer was dilated away from the WMH by 2 mm for a total of 7 NAWM layers. We then applied the WMH and NAWM L1 to L7 masks to the PET, CBF, FA, and MD maps, which were previously linearly aligned to their T1-weighted images (Figure 1). The mean CBF, FA, MD, and ^{68}Ga-NOTA-PRGD2 uptake for the WMH and each NAWM layer were measured; the surrounding brain tissue regions were excluded through the brain mask. Standardized uptake value ratios (SUV_r) were calculated for each NAWM layer, divided by the respective WMH.

Serological Test

Serum samples were collected from all participants and stored at −80 °C. The angiogenesis array (RayBiotech, Norcross, GA) was used to detect the serum concentrations of angiogenic factors, including E-selectin, matrix metalloproteinase (MMP)-2, MMP-9, vascular endothelial growth factor (VEGF) receptor 2, VEGF receptor 1, and VEGF-A. An ELISA was used to detect serum concentrations of integrin αvβ3 (LifeSpan BioSciences), S100B (LifeSpan BioSciences), and hypoxia-inducible factor 1-alpha (HIF-1 alpha) (RayBiotech).

Statistical Analysis

Baseline characteristics with normal distribution are reported as mean±SD. Nonnormally distributed variables are presented as medians (interquartile range). Independent-sample *t* tests or the Mann–Whitney *U* test were used for continuous variables, and chi-square tests were used for categorical variables to compare the differences between the 2 groups. We compared ^{68}Ga-NOTA-PRGD2 PET with SUV_r, CBF, FA, and MD in WMH and NAWM L1 to L7. The values from NAWM L7 were used as references. Structural penumbra was defined as the NAWM region with a reduced FA or MD. CBF penumbra was defined as

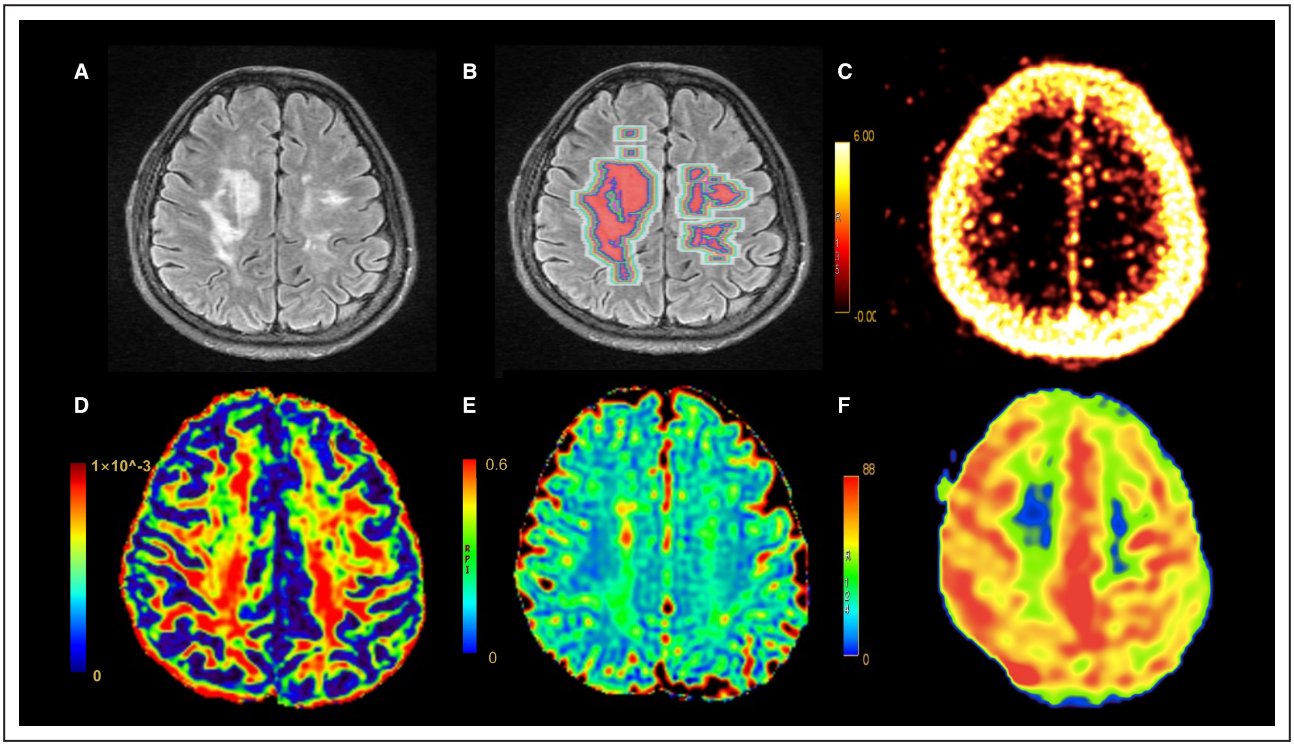

Figure 1. **^{68}Ga-NOTA-PRGD2 PET/MRI.**
A, FLAIR sequence showed WMHs at centrum semiovale. **B**, WMH and NAWM masks for each individual were created. Each NAWM layer was dilated away from the WMHs by 2 mm for a total of 7 NAWM layers. **C**, ^{68}Ga-NOTA-PRGD2 PET. **D**, The FA map. **E**, The MD map. **F**, The CBF map. CBF indicates cerebral blood flow; FA, fractional anisotropy; FLAIR, fluid attenuated inversion recovery; MD, mean diffusivity; MRI, magnetic resonance imaging; NAWM, normal-appearing white matter; PET, positron emission tomography; and WMHs, white matter hyperintensities.

the NAWM region with a reduced CBF.[8] The relationships among CBF, FA, MD, and SUV_r were assessed using Spearman's correlation analysis. The serum concentrations of angiogenic factors were compared between the 2 groups. Bonferroni correction was used to perform a correction for multiple comparisons. Standardized mean difference (SMD) and 95% CI were calculated. Analyses were performed using the Statistical Package for the Social Sciences version 25.0 software (SPSS; IBM, Armonk, NY). Statistical significance was set at P<0.05.

RESULTS

Twenty-one patients were included in this study. Demographic characteristics of the participants are presented in Table 1. The mean age of the study population was 55.3 (SD=14.2) years. The patients were classified into 2 groups on the basis of a median SUV_{max} threshold of 0.17. Patients with SUV_{max} ≤0.17 were classified as group 1. Patients with increased ^{68}Ga-NOTA-PRGD2 uptake (SUV_{max} >0.17) were classified into group 2. The patients in group 2 had a significantly higher SUV_{max} than those in group 1 (0.45±0.22 versus 0.06±0.08, P<0.001) (Figure 2).

Spatial Distribution of ^{68}Ga-NOTA-PRGD2 Uptake

We analyzed ^{68}Ga-NOTA-PRGD2 uptake in WMH, NAWM, and the border between WMH and NAWM. We found that ^{68}Ga-NOTA-PRGD2 uptake was more obvious on the border between the WMH and NAWM (Figure 3). In group 2, ^{68}Ga-NOTA-PRGD2 SUV_{max} was significantly higher than that of WMH (P=0.004). In group 1, the SUV_{max} was not significantly different among the 3 regions (Figure 4).

Figure 5A shows a comparison of ^{68}Ga-NOTA-PRGD2 uptake between the WMH and NAWM layers (L1–L7) in groups 1 and 2. ^{68}Ga-NOTA-PRGD2 SUV_r was significantly higher in NAWM L1 to L7 than in WMH (P<0.001) in group 2. However, there was no significant increase in ^{68}Ga-NOTA-PRGD2 SUV_r between WMH and NAWM L1 to L7 in group 1 (P=0.251).

Influencing Factors of Angiogenesis

Patients in group 2 had a larger WMH volume than those in group 1 (P=0.002) (Table 1). The serum levels of integrin αvβ3, VEGF receptor 2, and interleukin-1β were significantly higher in group 2 than in group 1 (P=0.038, P=0.03, and P=0.012, respectively). There were no significant differences in the serum levels of S100B and

Table 1. Summary of Participant Characteristics

	Total (n=21)	Group 1 (n=7)	Group 2 (n=14)
Age, y, mean±SD (range)	55.33±14.20 (25–79)	58.29±20.10 (25–79)	53.86±10.81 (31–66)
Sex, female, n (%)	15 (71.4%)	7 (100%)	8 (57.1%)
Hyperlipidemia, n (%)	8 (38.1%)	4 (57.1%)	4 (28.6%)
Hypertension, n (%)	16 (76.2%)	5 (71.4%)	10 (71.4%)
Diabetes, n (%)	3 (14.3%)	2 (28.6%)	1 (7.1%)
eGFR [mL/(min×1.73 m^2	95.43±29.14	84.25±22.40	101.46±31.33
MMSE score, mean (SD)	23.33±6.70	22.14±7.02	25.71±5.74
BPF, mean (SD)	0.70±0.07	0.73±0.09	0.69±0.06
WMH volume, mL, mean (SD)	41.80±30.88	17.56±15.30	53.92±29.73
Number of lacunes, median (IQR)	3 (1.5–8)	4 (2–5)	3 (1–10)
Number of CMBs, median (IQR)	10 (2.5–21)	6 (5–15)	12 (0.75–24)
Severe CSO-PVS, n (%)	15 (71.4%)	5 (71.4%)	10 (71.4%)
Severe BG-PVS, n (%)	8 (38.1%)	3 (42.9%)	5 (35.7%)
WMH SUV_{max}, mean (SD)	0.14±0.14	0.01±0.01	0.21±0.12
WMH-NAWM SUV_{max}, mean (SD)	0.29±0.24	0.03±0.05	0.41±0.19
NAWM SUV_{max}, mean (SD)	0.24±0.24	0.04±0.08	0.34±0.24

BG indicates basal ganglia; BPF, brain parenchymal fraction; CMBs, cerebral small-vessel diseases; CSO, centrum semiovale; eGFR, estimated glomerular filtration rate; MMSE, Mini-Mental State Examination; NAWM, normal-appearing white matter; PVS, perivascular spaces; SUV_{max}, maximum standardized uptake value; and WMH, white matter hyperintensity.

HIF-1α between the 2 groups (*P*=0.689 and *P*=0.062, respectively) (Table 2). After applying multiple comparisons to the number of tests, no significant associations were found between the 2 groups (*P*<0.05/13=0.004).

Serum levels of integrin αvβ3 were associated with WMH volume (*r*=0.545, *P*=0.011) and MMP-2 (*r*=0.689, *P*<0.001). In group 2 (n=14), serum levels of integrin αvβ3 were associated with WMH volume (*r*=0.648, *P*=0.012) and MMP-2 (*r*=0.731, *P*=0.003) (Figure 6A and 6B). In group 1 (n=7), SUV_{max} was associated with E-selectin (rho=0.875, *P*=0.010), interleukin-6 (rho=0.867, *P*=0.012), and S100B (rho=−0.835, *P*=0.019). In group 2, SUV_{max} was associated with WMH volume (*r*=−0.683, *P*=0.007) (Figure 6C).

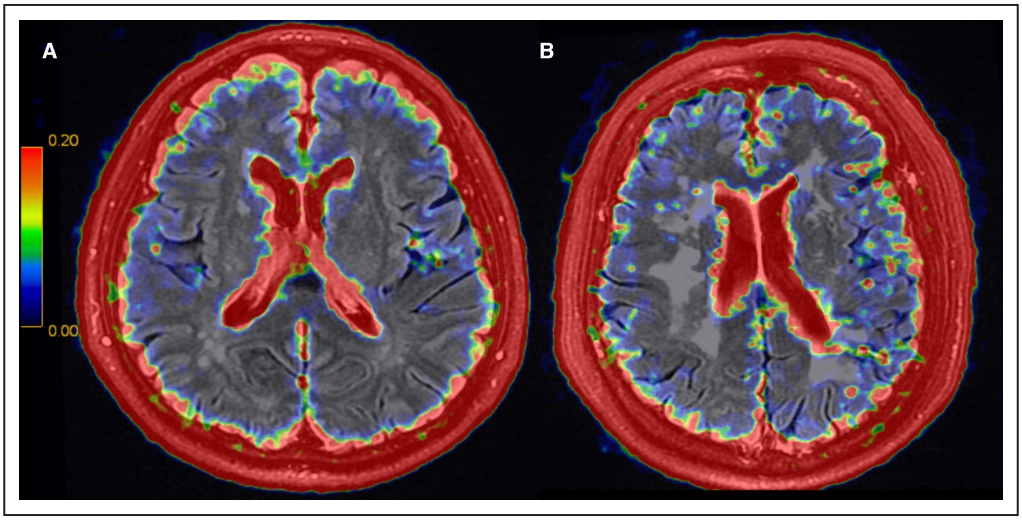

Figure 2. WMHs and ^{68}Ga-NOTA-PRGD2 uptake.
A, Example of a patient in group 1. The integrated PET/MRI of ^{68}Ga-NOTA-PRGD2 PET and FLAIR imaging show no significant increase in ^{68}Ga-NOTA-PRGD2 uptakes in WMH and NAWM. **B**, Example of a patient in group 2. The integrated PET/MRI of ^{68}Ga-NOTA-PRGD2 PET and FLAIR imaging show significantly increased ^{68}Ga-NOTA-PRGD2 uptakes in WMH and NAWM. FLAIR indicates fluid attenuated inversion recovery; MRI, magnetic resonance imaging; NAWM, normal-appearing white matter; PET, positron emission tomography; and WMHs, white matter hyperintensities.

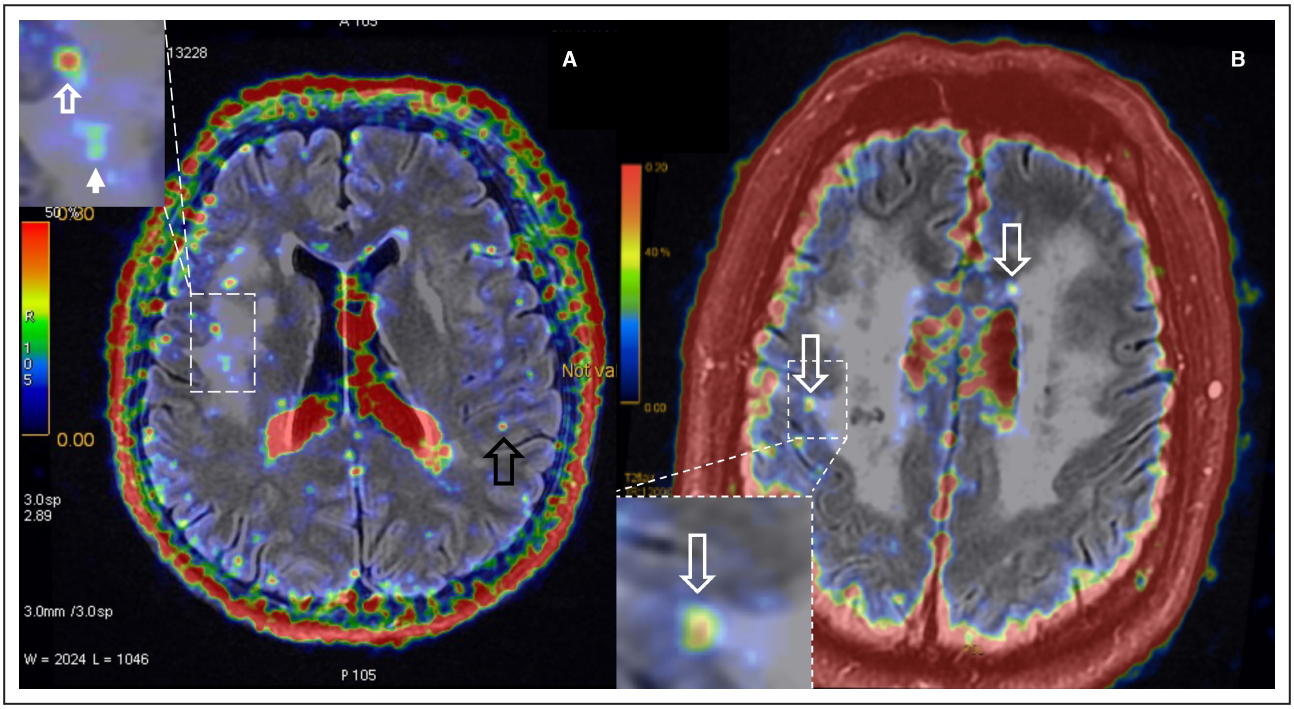

Figure 3. Distribution of ^{68}Ga-NOTA-PRGD2 uptake.
A, Example of a patient in group 2, the integrated PET/MRI of ^{68}Ga-NOTA-PRGD2 PET and FLAIR imaging show the pattern of ^{68}Ga-NOTA-PRGD2 uptakes in WMHs (solid white arrow), NAWM (faint black arrow), and the border of WMH and NAWM (faint white arrow). **B**, Example of a patient in group 2, the integrated PET/MRI of ^{68}Ga-NOTA-PRGD2 PET and FLAIR imaging show the pattern of ^{68}Ga-NOTA-PRGD2 uptakes in the border of WMH and NAWM (faint white arrow). FLAIR indicates fluid attenuated inversion recovery; MRI, magnetic resonance imaging; NAWM, normal-appearing white matter; PET, positron emission tomography; and WMHs, white matter hyperintensities.

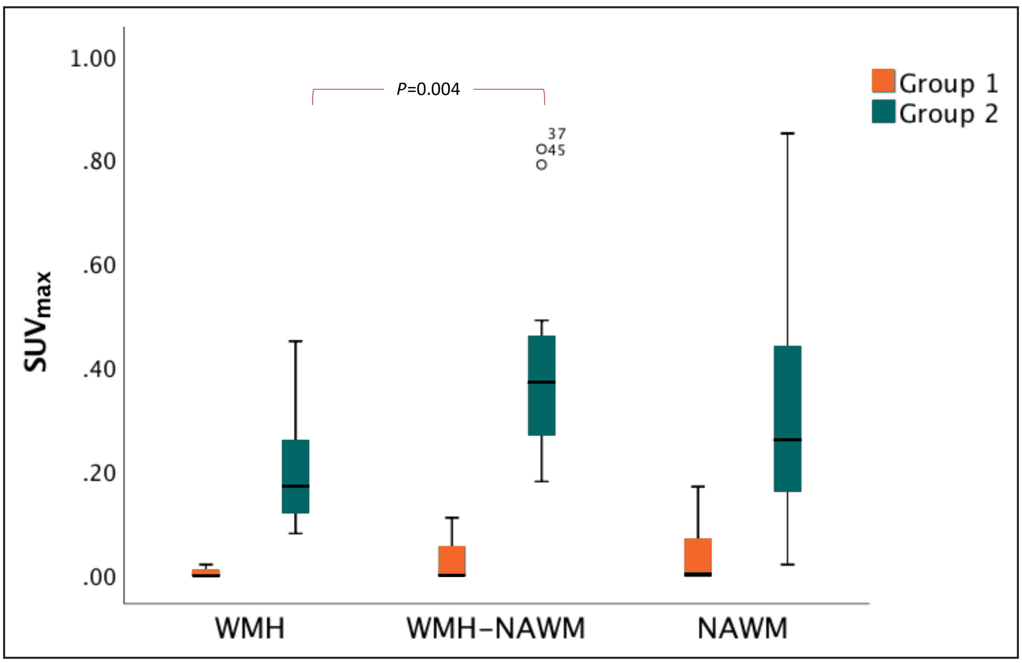

Figure 4. Spatial distribution of ^{68}Ga-NOTA-PRGD2 uptake.
^{68}Ga-NOTA-PRGD2 uptakes were significantly increased at the border of WMH and NAWM than in WMH in group 2. NAWM indicates normal-appearing white matter; SUV_{max}, maximum standardized uptake values; and WMH, white matter hyperintensities.

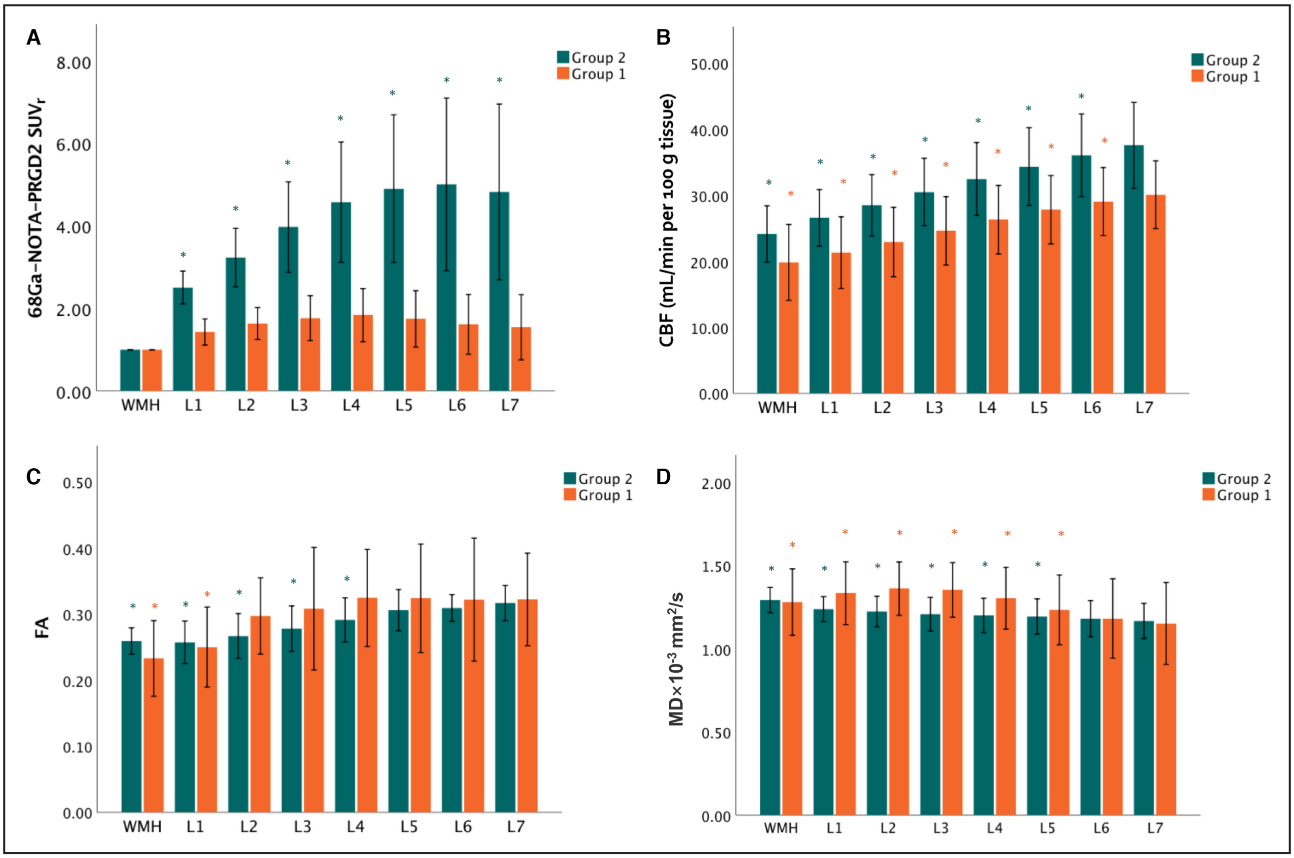

Figure 5. WMH penumbra.
A, The ^{68}Ga-NOTA-PRGD2 SUV_r was significantly increased in NAWM layers (L1–L7) than in WMHs in group 2. **B**, The mean CBF of WMHs and NAWM L1 to L6 was significantly lower than that of the NAWM L7 in groups 1 and 2. **C**, The mean FA of WMHs and NAWM L1 was significantly lower than that of NAWM L7 in group 1. The mean FA of WMHs and NAWM L4 was significantly lower than that of NAWM L7 in group 2. **D**, The MD of WMHs and NAWM L1 to L5 in groups 1 and 2. CBF indicates cerebral blood flow; FA, fractional anisotropy; MD, mean diffusivity; NAWM indicates normal-appearing white matter; SUV_r, standardized uptake value ratios; and WMHs, white matter hyperintensities.

Angiogenesis and CBF WMH Penumbra

For patients without significantly increased ^{68}Ga-NOTA-PRGD2 uptake (group 1), the mean CBF of WMH and NAWM L1 to L6 was significantly lower than that of NAWM L7 (P<0.001). For patients with significantly increased ^{68}Ga-NOTA-PRGD2 uptake (group 2), the mean CBF of WMH and NAWM L1 to L6 was also significantly lower than that of NAWM L7 (P<0.001) (Figure 5B). We further investigated the correlation between the mean CBF and ^{68}Ga-NOTA-PRGD2 uptake. The results showed a negative correlation between SUV_r and CBF in group 2 (r=−0.238, P=0.018). However, there was no significant correlation between SUV_r and CBF across different levels.

Angiogenesis and Structural WMH Penumbra

For patients without significantly increased ^{68}Ga-NOTA-PRGD2 uptake (group 1), the mean FA of WMH and NAWM L1 was significantly lower than that of NAWM L7 (P=0.005 and P=0.017, respectively) (Figure 5C). The mean MD of WMH and NAWM L1 to L5 was higher than that of NAWM L7 (P=0.004) (Figure 5D).

For patients with significantly increased ^{68}Ga-NOTA-PRGD2 uptake (group 2), a comparison between WMH and NAWM demonstrated that the mean FA of WMH and NAWM L1 to L4 was significantly lower than that of NAWM L7 (P<0.001) (Figure 3C). The mean MD of WMH and NAWM L1 to L5 was higher than that of NAWM L7 (P<0.001) (Figure 5D).

We investigated the correlation between white matter integrity and ^{68}Ga-NOTA-PRGD2 uptake. The results showed significant correlation between SUV_r and FA in group 2 (L2 [r=−0.552, P=0.041]; L3 [r=−0.684, P=0.007]; L4 [r=−0.741, P=0.002]; L5 [r=−0.789, P<0.001]; L6 (r=−0.798, P<0.001); L7 [r=−0.714, P=0.004]) (Figure 7). There was no significant correlation between SUV_r and MD in WMH and NAWM L1 to L7.

Table 2. Angiogenic and Inflammatory Factors

Factors (ng/mL)	Group 1	Group 2	*P* value	SMD (95% CI)
hs-CRP, mg/L	1.16±1.083	1.84±2.96	0.596	−0.68 (−3.18 to 1.81)
Interleukin-1β	0.01±0.01	0.04±0.07	0.012	−0.04 (−0.09 to 0.02)
Interleukin-6	0.02±0.02	0.09±0.25	0.743	−0.08 (−0.280 to 0.13)
Interleukin-8	0.01±0.02	0.04±0.06	0.636	−0.08 (−0.28 to 0.13)
E-selectin	3.00±4.14	4.06±3.40	0.36	−0.02 (−0.06 to 0.01)
VEGF-A	0.03±0.02	0.03±0.02	0.971	0.00 (−0.02 to 0.02)
Integrin αvβ3	0.32±0.26	0.58±0.30	0.038	−0.26 (−0.54 to 0.02)
MMP-2	0.81±0.45	1.61±1.11	0.085	−0.78 (−1.71 to 0.15)
MMP-9	7.85±1.71	8.07±3.24	0.873	−0.22 (−2.99 to 2.54)
VEGF receptor 2	8.10±1.64	1.09±3.77	0.030	−0.27 (−0.53 to 0.02)
VEGF receptor 1	0.47±0.32	0.61±0.25	0.269	−0.14 (−0.41 to 0.13)
HIF-1α	0.02±0.02	0.05±0.04	0.062	−0.03 (−0.061 to 0.00)
S100B	3.91±5.53	2.90±2.20	0.689	1.01 (−2.48 to 4.50)

HIF-1α indicates hypoxia-inducible factor-1 alpha; hs-CRP, high-sensitivity C-reactive protein; MMP, matrix metalloproteinase; SMD, standardized mean difference; and VEGF, vascular endothelial growth factor.

DISCUSSION

In this study, we found that angiogenesis was present in patients with WMH. A higher WMH burden is a predictive factor for angiogenesis in cerebral small-vessel disease. More specifically, we found that integrin αvβ3 expression was significantly increased on the border between the WMH and NAWM. These findings suggest that angiogenesis may occur in the WMH penumbra in patients with a high WMH burden.

Previous investigations have investigated the WMH penumbra in the NAWM tissue surrounding WMHs, which may represent a subtle vascular and neuronal injury.[5–8] In the present study, we found that the structural penumbras, as defined by FA and MD, were ≈2 to 10 mm surrounding the WMH; CBF penumbras, as defined by CBF, were ≈12 mm from WMH. These results are consistent with those of previous studies, which reported that the CBF penumbra was ≈11 to 14 mm surrounding the WMH, whereas the DTI-FA penumbra covered ≈2 to 9 mm from the WMH.[7,8] We observed that the structural penumbra was narrower in the group without significant angiogenesis and with lower WMH volume. Additionally, our results confirmed that the CBF penumbra was more extensive than the structural penumbra.

However, whether hypoxia promotes angiogenesis in the central nervous system remains unknown. Angiogenesis is a complex process that involves numerous factors. We found that serum levels of integrin αvβ3, VEGF receptor 2, and interleukin-1β were higher in the group with significantly increased ^{68}Ga-NOTA-PRGD2 uptake, indicating the regulatory effects of the angiogenic factors in this study. Previous studies have shown that cerebrospinal fluid biomarkers of angiogenesis, such as VEGF, VEGF receptor 1, VEGF receptor 2, and placental growth factor are associated with more pronounced white matter lesions in patients with Parkinson disease. Hypoperfusion and hypoxia associated with orthostatic hypotension have been proposed as potential mechanisms.[15] It is likely that the state of hypoperfusion and chronic ischemia that leads to the manifestation of WMH on brain MRI also acts as a trigger for the upregulation of angiogenic factors. Higher levels of intercellular adhesion molecule 1, E-selectin, neopterin, and vascular cell adhesion molecule 1 were observed in patients with greater WMH volumes and lacunar infarcts. Previous studies have also emphasized that interleukin-1β could have an impact on white matter lesions and angiogenesis.[24,25]

In this study, we found that both reduced CBF and microstructural integrity are correlated with angiogenesis. We hypothesized that compromised CBF precedes microstructural integrity changes and induces angiogenesis. Khan et al[26] reported that chronic remote ischemic conditioning can induce angiogenesis and cerebral vascular remodeling. Previous studies using animal models of chronic cerebral hypoperfusion have shown that bilateral common carotid artery stenosis–induced ischemic white matter damage is significantly improved after transplantation of bone marrow mononuclear cells through endothelial nitric oxide synthase activation, upregulation of the VEGF–VEGF receptor 2 signaling pathway, and subsequent angiogenesis.[27,28]

The WMH penumbra has been associated with expansion of the WMH. However, the causal relationship between the reduction in CBF and microstructural integrity with WMH progression remains controversial. The deep white matter is particularly susceptible to injury from hypoperfusion because this area is supplied exclusively by perforating arterioles arising from the leptomeningeal border zone and must travel a long distance to reach the deep white matter.[9,29–31]

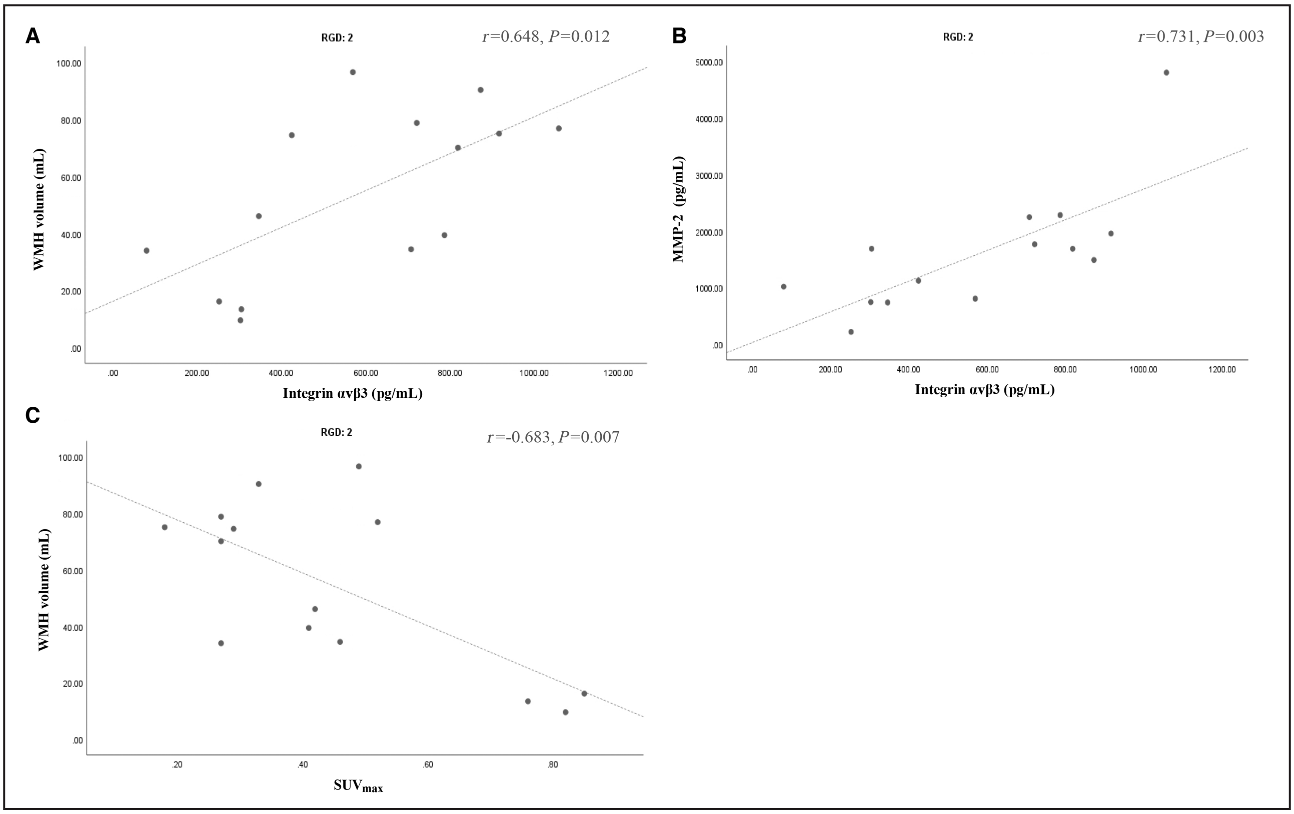

Figure 6. The correlation between angiogenesis with angiogenic factors and WMH volume.
A, The correlation between serum integrin αvβ3 and WMH volume in group 2. **B**, The correlation between serum integrin αvβ3 and MMP-2 in group 2. **C**, The correlation between SUV_{max} and WMH volume in group 2. MMP indicates matrix metalloproteinase; SUV_{max}, maximum standardized uptake value; and WMH, white matter hyperintensity.

Staffaroni et al[32] found that longitudinal low baseline CBF was associated with an increased WMH burden. Promjunyakul et al[33] found that baseline reduced CBF and microstructural characteristics of the WMH penumbra region were predictors of WMH growth, especially the inner 5 mm of the penumbra.

Whether angiogenesis in the WMH penumbra has an impact on WMH growth remains unknown. Ischemia-induced angiogenesis may be a possible mechanism to compensate for hypoperfusion in WMH and may be beneficial for remyelination and white matter tract rewiring. Recent studies have demonstrated that angiogenesis plays a beneficial role in accelerating white matter remodeling. Oligodendrocytes may secrete angiogenic factors, such as MMP-9, which accelerate angiogenesis and promote white matter remodeling after white matter injury.[25] In contrast, VEGF, MMPs, and other angiogenesis factors could lead to blood–brain barrier disruption.[14,34–36] Blood–brain barrier disruption is considered to play a role in the pathophysiology of WMH. However, we did not find significant differences in S100B levels in this study. Future studies using neuroimaging to precisely measure the blood–brain barrier will be more instructive.

This study is the first to provide in vivo evidence of an association between angiogenesis and WMH penumbra. We used a novel noninvasive method, ^{68}Ga-NOTA-PRGD2 PET/MRI, to detect angiogenesis in vivo. Nuclear medicine and molecular imaging are complementary imaging methods for a better understanding of the mechanisms underlying central nervous system diseases. Integrated PET/MRI enables the analysis of both anatomic structures and metabolic processes in cerebrovascular diseases. Furthermore, integrin αvβ3 has been a popular treatment modality for pro- or antiangiogenesis approaches. This insight will provide new therapeutic directions for cerebral small-vessel disease treatment.

This study has several limitations. First, our cross-sectional analysis did not prove causality. Further prospective studies are needed to verify the impact of angiogenesis on WMH growth. Second, our results were limited by the small sample size. The multiple comparisons may lead to a high rate of false negatives or false positives in such small sample size, and the possibility of residual confounding cannot be excluded. The results showed some floor effects and nonlinear associations between angiogenesis and structural WMH penumbra. Further study with a large sample size should be performed to prove the linear correlations. Third, in group 2 of patients with high WMH burden, the WMH penumbra and NAWM were closer to the cortex, which

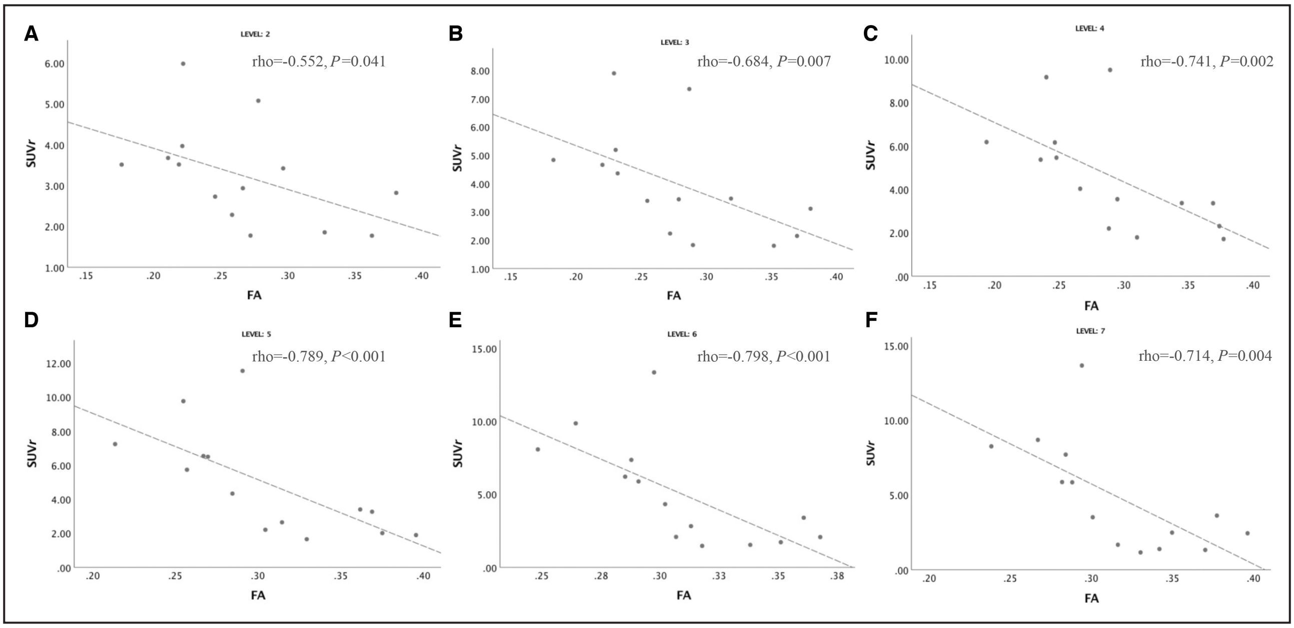

Figure 7. The correlation between ^{68}Ga-NOTA-PRGD2–SUV$_r$ and FA.
The ^{68}Ga-NOTA-PRGD2 SUV$_r$ was correlated with FA in NAWM layers (L2–L7) in group 2. FA indicates fractional anisotropy; NAWM, normal-appearing white matter; and SUV$_r$, standardized uptake value ratios.

may have induced relatively greater CBF values. Future studies with larger sample sizes should be conducted to analyze the differences in CBF penumbra in different locations, including deep WMH and periventricular WMH. Fourth, magnetic resonance attenuation correction was performed in this study, which disregards the potential influence of cortical bone. Previous studies have shown that magnetic resonance attenuation correction led to underestimation of PET values in comparison to computed tomography–based attenuation correction, which may explain the relatively low standardized uptake values in our study. However, the difference is typically <10%.[37,38] Besides, there are several advantages. Combined PET/MRI examinations may facilitate improvements in the additional use of magnetic resonance for retrospective motion correction or magnetic resonance–based partial volume correction of PET.[22] Finally, the integrity of the blood–brain barrier may affect ^{68}Ga-NOTA-PRGD2 uptakes. The consistency of ^{68}Ga-NOTA-PRGD2 uptakes and angiogenesis still needs to be confirmed by pathology study.

CONCLUSIONS

This study further defined the WMH penumbra pattern. Our results demonstrate that angiogenesis was present in the WMH penumbra. Additionally, our findings indicate that angiogenesis is correlated with reduced CBF and microstructural integrity. This study suggested the potential therapeutic value of angiogenesis in the prevention and treatment of WMH. Further studies are warranted to verify the important role of angiogenesis in the development of WMHs and integrin αvβ3-targeted molecular imaging as a noninvasive monitoring technique.

ARTICLE INFORMATION

Received October 20, 2022; accepted September 19, 2023.

Affiliations

Department of Neurology, Beijing Tiantan Hospital, Capital Medical University, Beijing, China (L.D.); China National Clinical Research Center for Neurological Diseases, Beijing, China (L.D.); Department of Radiology, Peking Union Medical College Hospital, Chinese Academy of Medical Science and Peking Union Medical College, Beijing, China (B.H., T.S., F.F.); Department of Nuclear Medicine (J.Z., Z.Z.) and Department of Neurology (B.P.), Peking Union Medical College Hospital, Chinese Academy of Medical Science and Peking Union Medical College, Beijing, China and Department of Neurology, State Key Laboratory of Complex Severe and Rare Diseases, Beijing, China (B.P.).

Acknowledgments

We acknowledge the significant contribution of the patients, families, and researchers.

Sources of Funding

This work was supported by the National Natural Science Foundation of China (Grant Nos. 81971137, 81750001, and 82101360) and the Chinese Academy of Medical Sciences Innovation Fund for Medical Sciences (Grant No. 2016-I2M-1-002).

Disclosures

None.

REFERENCES

1. Debette S, Markus HS. The clinical importance of white matter hyperintensities on brain magnetic resonance imaging: systematic review and meta-analysis. *BMJ*. 2010;341:c3666. doi: 10.1136/bmj.c3666

2. Schmidt R, Ropele S, Enzinger C, Petrovic K, Smith S, Schmidt H, Matthews PM, Fazekas F. White matter lesion progression, brain atrophy, and cognitive decline: the austrian stroke prevention study. *Ann Neurol*. 2005;58:610–616. doi: 10.1002/ana.20630
3. Lawrence AJ, Zeestraten EA, Benjamin P, Lambert CP, Morris RG, Barrick TR, Markus HS. Longitudinal decline in structural networks predicts dementia in cerebral small vessel disease. *Neurology*. 2018;90:e1898–e1910. doi: 10.1212/WNL.0000000000005551
4. Sabayan B, van der Grond J, Westendorp RG, van Buchem MA, de Craen AJ. Accelerated progression of white matter hyperintensities and subsequent risk of mortality: a 12-year follow-up study. *Neurobiol Aging*. 2015;36:2130–2135. doi: 10.1016/j.neurobiolaging.2015.03.003
5. Maillard P, Fletcher E, Harvey D, Carmichael O, Reed B, Mungas D, DeCarli C. White matter hyperintensity penumbra. *Stroke*. 2011;42:1917–1922. doi: 10.1161/STROKEAHA.110.609768
6. Maillard P, Fletcher E, Lockhart SN, Roach AE, Reed B, Mungas D, DeCarli C, Carmichael OT. White matter hyperintensities and their penumbra lie along a continuum of injury in the aging brain. *Stroke*. 2014;45:1721–1726. doi: 10.1161/STROKEAHA.113.004084
7. Promjunyakul N, Lahna D, Kaye JA, Dodge HH, Erten-Lyons D, Rooney WD, Silbert LC. Characterizing the white matter hyperintensity penumbra with cerebral blood flow measures. *Neuroimage Clin*. 2015;8:224–229. doi: 10.1016/j.nicl.2015.04.012
8. Promjunyakul NO, Lahna DL, Kaye JA, Dodge HH, Erten-Lyons D, Rooney WD, Silbert LC. Comparison of cerebral blood flow and structural penumbras in relation to white matter hyperintensities: a multimodal magnetic resonance imaging study. *J Cereb Blood Flow Metab*. 2016;36:1528–1536. doi: 10.1177/0271678X16651268
9. Pantoni L, Garcia JH. Pathogenesis of leukoaraiosis: a review. *Stroke*. 1997;28:652–659. doi: 10.1161/01.STR.28.3.652
10. Young VG, Halliday GM, Kril JJ. Neuropathologic correlates of white matter hyperintensities. *Neurology*. 2008;71:804–811. doi: 10.1212/01.wnl.0000319691.50117.54
11. Bernbaum M, Menon BK, Fick G, Smith EE, Goyal M, Frayne R, Coutts SB. Reduced blood flow in normal white matter predicts development of leukoaraiosis. *J Cereb Blood Flow Metab*. 2015;35:1610–1615. doi: 10.1038/jcbfm.2015.92
12. Font MA, Arboix A, Krupinski J. Angiogenesis, neurogenesis and neuroplasticity in ischemic stroke. *Curr Cardiol Rev*. 2010;6:238–244. doi: 10.2174/157340310791658802
13. Krupinski J, Kaluza J, Kumar P, Kumar S, Wang JM. Role of angiogenesis in patients with cerebral ischemic stroke. *Stroke*. 1994;25:1794–1798. doi: 10.1161/01.STR.25.9.1794
14. Nakaji K, Ihara M, Takahashi C, Itohara S, Noda M, Takahashi R, Tomimoto H. Matrix metalloproteinase-2 plays a critical role in the pathogenesis of white matter lesions after chronic cerebral hypoperfusion in rodents. *Stroke*. 2006;37:2816–2823. doi: 10.1161/01.STR.0000244808.17972.55
15. Janelidze S, Lindqvist D, Francardo V, Hall S, Zetterberg H, Blennow K, Adler CH, Beach TG, Serrano GE, van Westen D, et al. Increased csf biomarkers of angiogenesis in parkinson disease. *Neurology*. 2015;85:1834–1842. doi: 10.1212/WNL.0000000000002151
16. Golestani R, Mirfeizi L, Zeebregts CJ, Westra J, de Haas HJ, Glaudemans AW, Koole M, Luurtsema G, Tio RA, Dierckx RA, et al. Feasibility of [18f]-RGD for ex vivo imaging of atherosclerosis in detection of alphavbeta3 integrin expression. *J Nucl Cardiol*. 2015;22:1179–1186. doi: 10.1007/s12350-014-0061-8
17. Jin ZH, Furukawa T, Claron M, Boturyn D, Coll JL, Fukumura T, Fujibayashi Y, Dumy P, Saga T. Positron emission tomography imaging of tumor angiogenesis and monitoring of antiangiogenic efficacy using the novel tetrameric peptide probe 64Cu-cyclam-RAFT-c(-RGDFK-)4. *Angiogenesis*. 2012;15:569–580. doi: 10.1007/s10456-012-9281-1
18. Menichetti L, Kusmic C, Panetta D, Arosio D, Petroni D, Matteucci M, Salvadori PA, Casagrande C, L'Abbate A, Manzoni L. MicroPET/CT imaging of alphavbeta(3) integrin via a novel (6)(8)Ga-NOTA-RGD peptidomimetic conjugate in rat myocardial infarction. *Eur J Nucl Med Mol Imaging*. 2013;40:1265–1274. doi: 10.1007/s00259-013-2432-9
19. Li D, Zhang J, Ji N, Zhao X, Zheng K, Qiao Z, Li F, Lang L, Iagaru A, Niu G, et al. Combined 68ga-NOTA-PRGD2 and 18f-FDG PET/CT can discriminate uncommon meningioma mimicking high-grade glioma. *Clin Nucl Med*. 2018;43:648–654. doi: 10.1097/RLU.0000000000002233
20. Shu S, Zhang L, Zhu YC, Li F, Cui LY, Wang H, Sun Y, Wu PL, Zhu ZH, Peng B. Imaging angiogenesis using (68)Ga-NOTA-PRGD2 positron emission tomography/computed tomography in patients with severe intracranial atherosclerotic disease. *J Cereb Blood Flow Metab*. 2017;37:3401–3408. doi: 10.1177/0271678X17696322
21. Sun Y, Zeng Y, Zhu Y, Feng F, Xu W, Wu C, Xing B, Zhang W, Wu P, Cui L, et al. Application of (68)Ga-PRGD2 PET/CT for alphavbeta3-integrin imaging of myocardial infarction and stroke. *Theranostics*. 2014;4:778–786. doi: 10.7150/thno.8809
22. Hofmann M, Pichler B, Scholkopf B, Beyer T. Towards quantitative PET/MRI: a review of MR-based attenuation correction techniques. *Eur J Nucl Med Mol Imaging*. 2009;36:S93–S104. doi: 10.1007/s00259-008-1007-7
23. Lin T, Qu J, Zuo Z, Fan X, You H, Feng F. Test-retest reliability and reproducibility of long-label pseudo-continuous arterial spin labeling. *Magn Reson Imaging*. 2020;73:111–117. doi: 10.1016/j.mri.2020.07.010
24. Didier N, Romero IA, Creminon C, Wijkhuisen A, Grassi J, Mabondzo A. Secretion of interleukin-1beta by astrocytes mediates endothelin-1 and tumour necrosis factor-alpha effects on human brain microvascular endothelial cell permeability. *J Neurochem*. 2003;86:246–254. doi: 10.1046/j.1471-4159.2003.01829.x
25. Pham LD, Hayakawa K, Seo JH, Nguyen MN, Som AT, Lee BJ, Guo S, Kim KW, Lo EH, Arai K. Crosstalk between oligodendrocytes and cerebral endothelium contributes to vascular remodeling after white matter injury. *Glia*. 2012;60:875–881. doi: 10.1002/glia.22320
26. Khan MB, Hafez S, Hoda MN, Baban B, Wagner J, Awad ME, Sangabathula H, Haigh S, Elsalanty M, Waller JL, et al. Chronic remote ischemic conditioning is cerebroprotective and induces vascular remodeling in a vcid model. *Transl Stroke Res*. 2018;9:51–63. doi: 10.1007/s12975-017-0555-1
27. Fujita Y, Ihara M, Ushiki T, Hirai H, Kizaka-Kondoh S, Hiraoka M, Ito H, Takahashi R. Early protective effect of bone marrow mononuclear cells against ischemic white matter damage through augmentation of cerebral blood flow. *Stroke*. 2010;41:2938–2943. doi: 10.1161/STROKEAHA.110.596379
28. Wang J, Fu X, Jiang C, Yu L, Wang M, Han W, Liu L, Wang J. Bone marrow mononuclear cell transplantation promotes therapeutic angiogenesis via upregulation of the VEGF-VEGFR2 signaling pathway in a rat model of vascular dementia. *Behav Brain Res*. 2014;265:171–180. doi: 10.1016/j.bbr.2014.02.033
29. Brown WR, Moody DM, Thore CR, Challa VR, Anstrom JA. Vascular dementia in leukoaraiosis may be a consequence of capillary loss not only in the lesions, but in normal-appearing white matter and cortex as well. *J Neurol Sci*. 2007;257:62–66. doi: 10.1016/j.jns.2007.01.015
30. Brown WR, Thore CR. Review: cerebral microvascular pathology in ageing and neurodegeneration. *Neuropathol Appl Neurobiol*. 2011;37:56–74. doi: 10.1111/j.1365-2990.2010.01139.x
31. Moody DM, Thore CR, Anstrom JA, Challa VR, Langefeld CD, Brown WR. Quantification of afferent vessels shows reduced brain vascular density in subjects with leukoaraiosis. *Radiology*. 2004;233:883–890. doi: 10.1148/radiol.2333020981
32. Staffaroni AM, Cobigo Y, Elahi FM, Casaletto KB, Walters SM, Wolf A, Lindbergh CA, Rosen HJ, Kramer JH. A longitudinal characterization of perfusion in the aging brain and associations with cognition and neural structure. *Hum Brain Mapp*. 2019;40:3522–3533. doi: 10.1002/hbm.24613
33. Promjunyakul NO, Dodge HH, Lahna D, Boespflug EL, Kaye JA, Rooney WD, Silbert LC. Baseline NAWM structural integrity and CBF predict periventricular WMH expansion over time. *Neurology*. 2018;90:e2119–e2126. doi: 10.1212/WNL.0000000000005684
34. Sun J, Yu L, Huang S, Lai X, Milner R, Li L. Vascular expression of angiopoietin1, alpha5beta1 integrin and tight junction proteins is tightly regulated during vascular remodeling in the post-ischemic brain. *Neuroscience*. 2017;362:248–256. doi: 10.1016/j.neuroscience.2017.08.040
35. Yang Y, Kimura-Ohba S, Thompson JF, Salayandia VM, Cosse M, Raz L, Jalal FY, Rosenberg GA. Vascular tight junction disruption and angiogenesis in spontaneously hypertensive rat with neuroinflammatory white matter injury. *Neurobiol Dis*. 2018;114:95–110. doi: 10.1016/j.nbd.2018.02.012
36. Zhang CE, Wong SM, van de Haar HJ, Staals J, Jansen JF, Jeukens CR, Hofman PA, van Oostenbrugge RJ, Backes WH. Blood-brain barrier leakage is more widespread in patients with cerebral small vessel disease. *Neurology*. 2017;88:426–432. doi: 10.1212/WNL.0000000000003556
37. Izquierdo-Garcia D, Sawiak SJ, Knesaurek K, Narula J, Fuster V, Machac J, Fayad ZA. Comparison of MR-based attenuation correction and CT-based attenuation correction of whole-body PET/MR imaging. *Eur J Nucl Med Mol Imaging*. 2014;41:1574–1584. doi: 10.1007/s00259-014-2751-5
38. Kops ER, Herzog H. Alternative methods for attenuation correction for pet images in MR-PET scanners. *2007 IEEE Nuclear Science Symposium Conference Record*. 2007;6:4327–4330.